arXiv:1302.2967v1 [astro-ph.CO] 13 Feb 2013

Possible Evidence of Thermodynamic Activity in Dark Matter Haloes

Sanjoy K. Sarker* and Allen Stern†

Department of Physics, University of Alabama,
Tuscaloosa, Alabama 35487, USA

ABSTRACT

We first deduce the density profiles and gravitational potential functions in the haloes of four galaxies (NGC 2403, NGC 2841, NGC 3521 and NGC 5055) using the rotation velocity data from THINGS. The analysis only requires that spherical symmetry is valid far from the disk. We find that the density decreases exponentially with the potential in substantial regions of the halo far from the disk, in agreement with the description of a single-component isothermal Boltzmann gas. We then compare the rotational velocity data with that obtained from solutions of the Poisson equation for a self-gravitating isothermal Boltzmann gas in regions $r > R_{\mathtt{G}}$ of the halo, r denoting the distance from the galactic origin. The minimum radius $R_{\mathtt{G}}$ can be varied, and good fits are obtained for a range of values for $R_{\mathtt{G}}$. Finally, for each galactic halo, we make three independent determinations of a constant for the Boltzmann gas, namely, the particle mass divided by the temperature, and find the results to be in general agreement.

---

* ssarker@bama.ua.edu

†astern@bama.ua.edu

1 Introduction

It is well known that a self-gravitating isothermal Boltzmann gas leads to flat rotation curves in the large distance limit, which is in qualitative agreement with the observed behavior in dark matter haloes. Despite this, thermodynamics is not normally considered in the treatment of dark matter haloes - the reason being that relaxation times arising from gravitational interactions alone are too long (compared with the Hubble time) for thermodynamic equilibrium to be established. Furthermore, if interactions other than gravity are present among the dark matter particles, they are generally believed to be too weak to establish thermal equilibrium.

On the other hand, if observations of galactic haloes are consistent with a Boltzmann description for the dark matter gas, the possibility of thermal equilibrium cannot be ruled out. It is therefore important to examine whether there is any quantitative agreement between dark matter haloes and the system of an isothermal gas. This is the purpose of the article. In section 2, we determine the density ρ in the halo as a function of the gravitational potential ϕ for four galaxies from rotation velocity data. (Here we only assume spherical symmetry, and do not make any á priori assumptions of thermal equilibrium). We find that there are significant regions in the haloes of these galaxies, where to a good approximation, ρ decreases exponentially with ϕ, in agreement with what one has for an isothermal Boltzmann gas. In section 3, we fit the rotation curve data for these galaxies to the solutions for a self-gravitating isothermal gas, and obtain qualitative results similar to those in section 2. From the results of sections 2 and 3 we can make three independent determinations of the relative temperatures of the galactic haloes, which are summarized and discussed in section 4.

In both sections 2 and 3, we make the simplifying assumption of spherical symmetry, which is reasonable at large enough distances from the disk. In section 3 we make the approximation of a single-component gas in the halo. We should then study galactic haloes for which these are reasonable approximations. The four galaxies we examine in this article are NGC 2403, NGC 2841, NGC 3521 and NGC 5055, and we use the rotation velocity data from THINGS[1]. These examples have the advantage that data is available at distances far beyond the quoted distance scale of the disk where spherical symmetry should be a good approximation. In addition, the quoted HI gas mass for these galaxies is a small percentage of the disk mass, which should lead to only small corrections in the halo due to the HI gas.

2 Direct determination of $\rho(\phi)$

Upon assuming spherical symmetry in the halo, the density ρ is a function of a single quantity, which we can choose to be the gravitational potential ϕ. In this section, we determine $\rho(\phi)$ directly from knowledge of rotation velocity data. This only requires Newtonian mechanics. The potential expressed as a function of the distance r from the galactic center is obtained the from speed $v(r)$ of orbiting objects by integrating

$$\frac{d\phi}{dr} = \frac{v(r)^2}{r} \;, \tag{1}$$

while the density is obtained from the Poisson equation

$$\rho(r) = \frac{1}{4\pi G r^2}\frac{d}{dr}\Big(r^2\frac{d\phi}{dr}\Big) = \frac{1}{4\pi G r^2}\frac{d}{dr}\Big(r v(r)^2\Big) \;, \tag{2}$$

where G is the gravitational constant. $\rho(\phi)$ is then recovered by comparing (1) and (2). We note that, since $\rho(r)$ is a single-valued function, so is $\rho(\phi)$. This follows because, from (1), ϕ is a monotonically increasing function of r. After obtaining the function $\rho(\phi)$ for different galactic haloes, it is then of interest to search for any universal behavior.

Below we numerically find $\rho(\phi)$ for the haloes of the four galaxies NGC 2403, NGC 2841, NGC 3521 and NGC 5055, using (1), (2) and the rotation velocity data from THINGS[1]. This is facilitated by first writing down a smooth function $v(r)$ that fits of the data to a finite series, for some specified range of the radial coordinate. We find that there are significant regions in the haloes, where to a good approximation, the numerically determined function $\rho(\phi)$ decreases exponentially, i.e,

$$\rho(\phi) = \rho_0 e^{-\frac{m\phi}{\Delta}}, \tag{3}$$

where ρ_0, m and Δ are constants. Such a result is identical to what one would obtain from a Boltzmann gas in thermal equilibrium, where m is the particle mass and the effective temperature is given by $T = \Delta/k_B$, k_B denoting the Boltzmann constant. As is well known, (3) is easily recovered in the ideal case where v =constant. There, ϕ varies logarithmically in r and $\rho(r) \propto r^{-2}$.[2] Here, we find that (3) is a good approximation in regions of galactic haloes where v *is not constant.* We are then able to extract approximate values for the ratio m/T for the four galactic haloes.

We begin with NGC 2841, and repeat the analysis for the remaining three galaxies.

NGC 2841

THINGS rotation velocity data for NGC 2841 is available at distances up to 51.6 kpc, which is far beyond the distance scale of the disk, 3.5 kpc[3]. The HI gas mass for NGC 2841 is $8.6 \times 10^9\ M_\odot$.[5] This is approximately 4% of the disk mass of $1.9552 \times 10^{11}\ M_\odot$, and so it should lead to only a small contribution in the halo.

A fit of the rotation velocity data to the series $\sum_{n=-3}^{4} a_n r^n$ from $r = 3.8$ to 51.6 kpc appears in figure 1. The fits are done to the midpoints of the error bars, corresponding to the dots in the figure. The gravitational potential, expressed as a function of r, is obtained by numerically integrating (1), and shown in figure 2. The density profile $\rho(r)$ is found using (2), and shown in figure 3. The latter two plots are combined in figure 4 to give $\log(\rho(\mathrm{r})/\mathrm{constant})$ versus $\phi(r)$. An approximate straight line is recovered upon restricting the radial coordinate to $7 < r < 22$ kpc, as is shown in the inset in figure 4. The slope of the latter is approximately -2.46×10^{-11} kg/J, which corresponds to $m/T \sim 191$ eV/^{o}K.

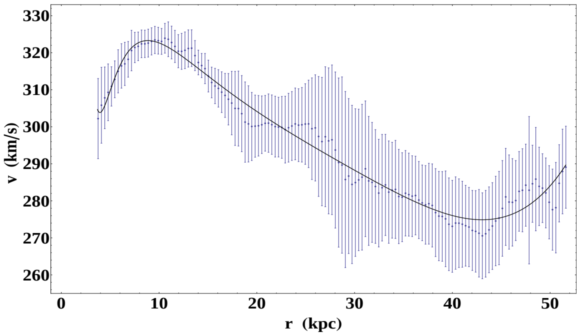

Figure 1: Series fit of rotation velocity data for NGC 2841 from $r = 3.8$ to 51.6 kpc.

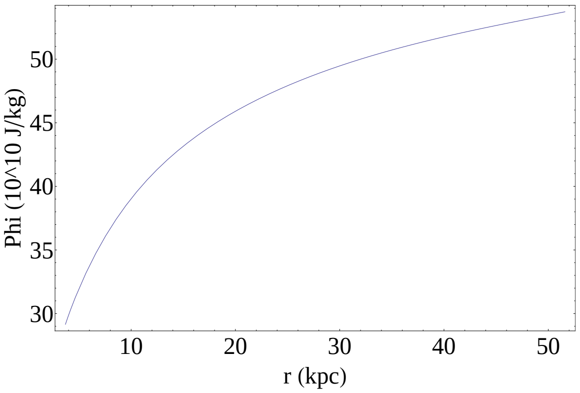

Figure 2: Resulting gravitational potential versus r for NGC 2841 from $r = 3.8$ to 51.6 kpc.

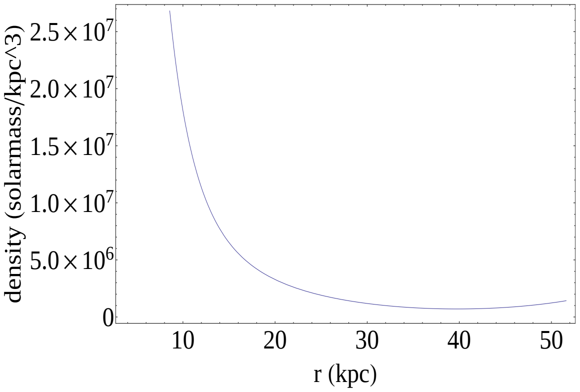

Figure 3: Resulting density versus r for NGC 2841 from $r = 3.8$ to 51.6 kpc.

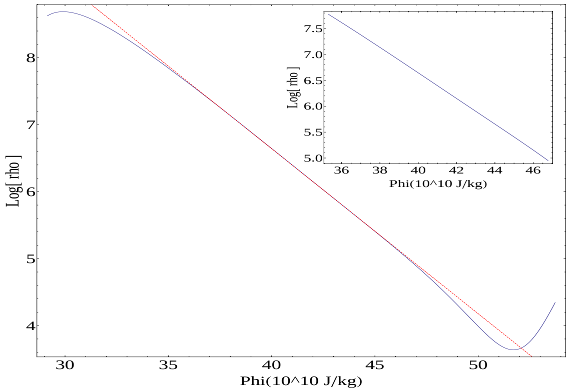

Figure 4: log (density/constant) versus the gravitational potential for NGC 2841 for $r = 3.8$ to 51.6 kpc. It is compared to a straight line (red, dashed) with slope $\approx -2.46 \times 10^{-11}$ kg/J, which corresponds to $m/T \sim 191$ eV/^{o}K. The radial coordinate is restricted to $7 < r < 22$ kpc in the inset.

NGC 5055

The distance scale of the disk for NGC 5055 is 3.622 kpc,[3] while THINGS rotation velocity data is available at distances up to 44.4 kpc. The HI gas mass for NGC 5055 is $.76 \times 10^{10}$ $M_\odot$,[5] which is approximately 12.6% of the disk mass of 6.035×10^{10} $M_\odot$. A series fit (again using $\sum_{n=-3}^{4} a_n r^n$) of the rotation velocity data from $r = .2$ to 44.4 kpc appears in figure 5, and the resulting plot of $\log(\rho(\mathrm{r})/\mathrm{constant})$ versus $\phi(r)$ is given in figure 6. An approximate straight line is recovered upon restricting the radial coordinate to $10 < r < 25$ kpc, as is shown in the inset in figure 6. The slope of the latter is approximately -5.71×10^{-11} kg/J, which corresponds to $m/T \sim 443$ eV/^{o}K.

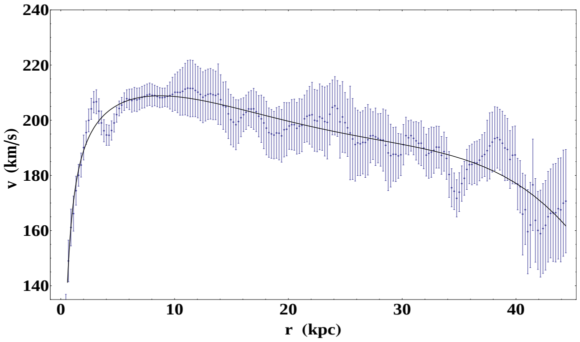

Figure 5: Series fit of rotation velocity data for NGC 5055 from $r = .2$ to 44.4 kpc.

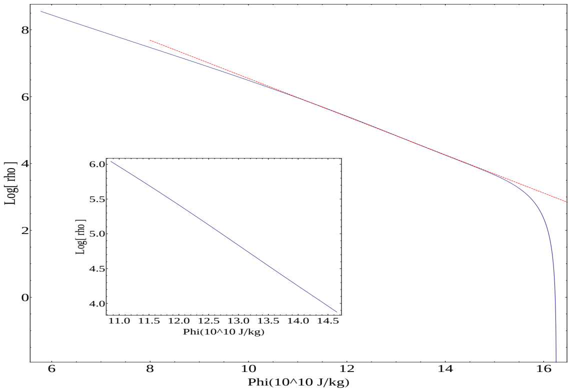

Figure 6: $\log(\mathrm{density}/\mathrm{constant})$ versus the gravitational potential for NGC 5055 for $r = 3$ to 44 kpc. It is compared to a straight line (red, dashed) with slope $\approx -5.71 \times 10^{-11}$ kg/J, which corresponds to $m/T \sim 443$ eV/^{o}K. The radial coordinate is restricted to $10 < r < 25$ kpc in the inset.

NGC 3521

The distance scale of the disk for NGC 3521 is 3.3 kpc,[3] while THINGS rotation velocity data is available at distances up to 35.5 kpc. The HI gas mass for NGC 3521 is 1.03×10^{10} $M_\odot$,[5] which is approximately 11% of the disk mass of 9.245×10^{10} $M_\odot$. A series fit of rotation velocity data from $r = 3.2$ to 35.5 kpc appears in figure 7, and the resulting plot of log $(\rho(\mathrm{r})/\mathrm{constant})$ versus $\phi(r)$ is given in figure 8. An approximate straight line is recovered upon restricting the radial coordinate to $7 < r < 15$ kpc, and is shown in the inset in figure 8. The slope of the latter is approximately -4.95×10^{-11} kg/J, which corresponds to $m/T \sim 384$ eV/^{o}K.

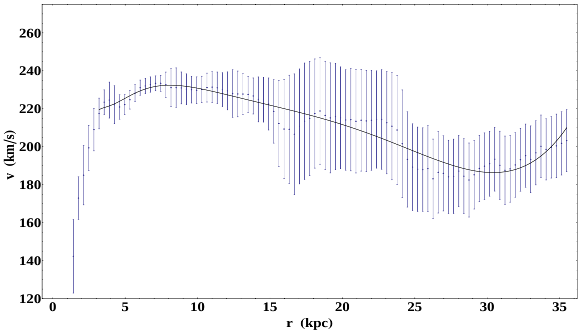

Figure 7: Series fit of rotation velocity data for NGC 3521 from $r = 3.2$ to 35.5 kpc.

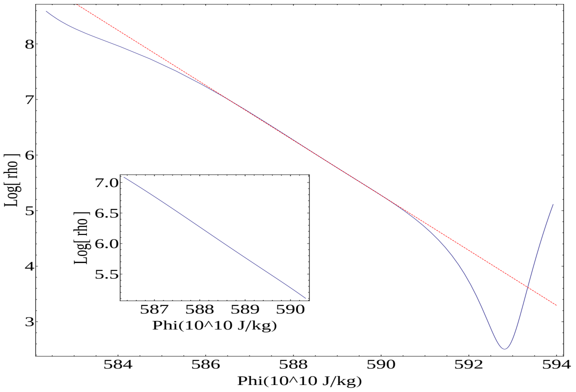

Figure 8: log (density/constant) versus the gravitational potential for NGC 3521 for $r = 3.2$ to 35.5 kpc. It is compared to a straight line (red, dashed) with slope $\approx -4.95 \times 10^{-11}$ kg/J, which corresponds to $m/T \sim 384$ eV/^{o}K. The radial coordinate is restricted to $7 < r < 15$ kpc in the inset.

NGC 2403

The distance scale of the disk for NGC 2403 is 2.75 kpc,[3] while THINGS rotation velocity data is available at distances up to 24 kpc. The HI gas mass for NGC 2841 is $4.6 \times 10^9\ M_\odot$,[5] which is approximately 19% of the disk mass of $2.37 \times 10^{10}\ M_\odot$. A series fit of rotation velocity data from $r = .1$ to 24 kpc appears in figure 7, and the resulting plot of $\log(\rho(\mathrm{r})/\mathrm{constant})$ versus $\phi(r)$ is given in figure 8. An approximate straight line is recovered upon restricting the radial coordinate to $3 < r < 10$ kpc, as is shown in the inset in figure 8. The slope of the latter is approximately -1.4×10^{-10} kg/J, which corresponds to $m/T \sim 1085$ eV/^{o}K.

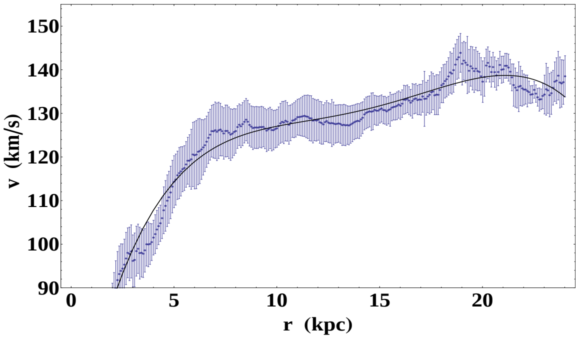

Figure 9: Series fit of rotation velocity data for NGC 2403 from $r = .1$ to 24 kpc.

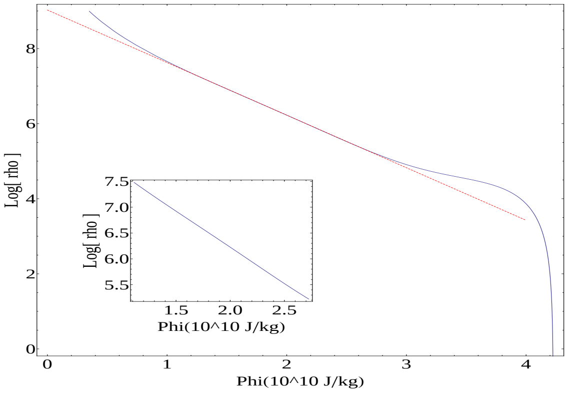

Figure 10: log (density/constant) versus the gravitational potential for NGC 2403 for $r = 1$ to 24 kpc. It is compared to a straight line (red, dashed) with slope $\approx -1.4 \times 10^{-10}$ kg/J, which corresponds to $m/T \sim 1085$ eV/^{o}K. The radial coordinate is restricted to $3 < r < 10$ kpc in the inset.

3 Boltzmann fits

As we have seen in section 2, the relation (3) approximately holds in sizable regions of the examined galactic haloes. It is then reasonable to compare the rotational velocity data with that obtained from a self-gravitating isothermal Boltzmann gas. With this in mind, we find solutions to the Poisson equation, where (3) is assumed for the dark matter density. We then fit the resulting rotation velocity curve $v(r)$ to the rotation velocity data from THINGS[1]. As in section 2, we shall assume spherical symmetry. Then for a single-component isothermal gas,

$$\frac{1}{r^2}\frac{d}{dr}\Big(r^2\frac{d\phi}{dr}\Big) \; = \; 4\pi G\rho_0 e^{-\frac{m\phi(r)}{k_B T}} \tag{4}$$

This is known as the Emden equation.[4] Here we assume that it is valid beyond some radius $R_{\mathtt{G}}$, but not necessarily for $r < R_{\mathtt{G}}$. The value of $R_{\mathtt{G}}$ must be sufficiently large compared to the disk radius so that deviations from spherical symmetry and contributions of the baryonic matter to the density in the right-hand-side of (4) can be ignored. The gravitational coupling of dark matter to the matter (both baryonic and nonbaryonic) within the sphere of radius $R_{\mathtt{G}}$ can be taken into account through boundary conditions imposed at $R_{\mathtt{G}}$. One of these conditions involves the acceleration of gravity $\frac{d\phi}{dr}$ at $r = R_{\mathtt{G}}$, which is determined by the total mass $M(R_{\mathtt{G}})$ in the region $0 < r \leq R_{\mathtt{G}}$. On the other hand, the value of ϕ at $r = R_{\mathtt{G}}$ is arbitrary. It is convenient to choose it to be zero so that ρ_0 is the mass density of the gas at $R_{\mathtt{G}}$, $\rho_0 = \rho(R_{\mathtt{G}})$. The boundary conditions then read[2]

$$\phi(R_{\mathtt{G}}) = 0 \qquad\qquad \frac{d\phi}{dr}\Big|_{r=R_{\mathtt{G}}} = \frac{GM(R_{\mathtt{G}})}{R_G^2} \tag{5}$$

From the solutions for $\phi(r)$, one can apply (1) to obtain the rotational speed v of an object in a circular orbit as a function of r. After fixing a value for R_G, the solution to (4) with boundary conditions (5), and hence $v(r)$, are determined by three parameters, which can be chosen to be m/T, $\rho(R_{\mathtt{G}})$ and $M(R_{\mathtt{G}})$.

Conversely, from observed rotational curve data one can do a three-parameter fit to the isothermal Boltzmann gas and determine m/T, $\rho(R_{\mathtt{G}})$ and $M(R_{\mathtt{G}})$ for any given $R_{\mathtt{G}}$. We shall do this below for the same four galactic haloes studied in section 2. Moreover, it is worthwhile to repeat the fits for a range of values of the initial radius $R_{\mathtt{G}}$. As m/T is a constant for a true isothermal gas Boltzmann, we can see how much the fitted values of m/T vary for different $R_{\mathtt{G}}$. The results can also be compared with the values for m/T obtained for the different galactic haloes in section 2. In addition, from the fitted values of $\rho(R_{\mathtt{G}})$ and $M(R_{\mathtt{G}})$ for different $R_{\mathtt{G}}$, we can recover the density profile and gravitational potential as a function of $R_{\mathtt{G}}$. We can then check if the boundary conditions found from the fits are consistent with an isothermal Boltzmann gas by plotting the log of $\rho(R_{\mathtt{G}})$ versus the gravitational potential derived from $M(R_{\mathtt{G}})$. This provides yet another determination of m/T for the halo, which can be compared with the previous results. We again begin with NGC 2841 and repeat the analysis for the remaining three galaxies.

NGC 2841

In section 2, Boltzmann gas-like behavior was observed for the galactic halo of NGC 2841 in the region $7 < r < 22$ kpc. Here we fit the rotation velocity data to the Boltzmann gas in the region $R_{\mathtt{G}} \leq r \leq 51.6$ kpc, where we allow the minimum radius $R_{\mathtt{G}}$ to vary from 7.18 kpc to 15 kpc. Due to the size of the error bars in the rotation velocity data, fits do not appear to be reliable if we increase the minimum radius $R_{\mathtt{G}}$ beyond 15 kpc. We exhibit the fits to a Boltzmann gas for $R_{\mathtt{G}} = 7.18$ and 13.67 kpc in figures 11 and 12, respectively. The results for the fits are $m/T = 193$ eV/^{o}K,

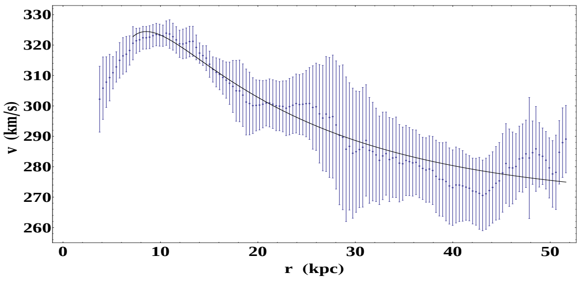

Figure 11: The results for the three-parameter fit of NGC 2841 rotation velocity data for $R_{\mathtt{G}} = 7.18$ kpc are: $m/T = 193$ eV/^{o}K, $\rho(R_{\mathtt{G}}) = 4.2 \times 10^7\ M_\odot/\text{kpc}^3$ and $M(R_{\mathtt{G}}) = 1.7 \times 10^{11}\ M_\odot$.

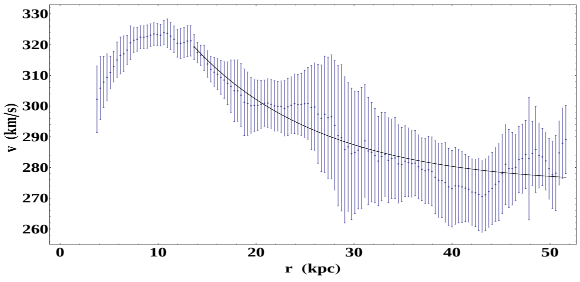

Figure 12: The results for the three-parameter fit of NGC 2841 rotation velocity data for $R_{\mathtt{G}} = 13.67$ kpc are: $m/T = 180$ eV/^{o}K, $\rho(R_{\mathtt{G}}) = 7.15 \times 10^6\ M_\odot/\text{kpc}^3$ and $M(R_{\mathtt{G}}) = 3.24 \times 10^{11}\ M_\odot$.

$\rho(R_{\mathtt{G}}) = 4.2 \times 10^7\ M_\odot/\text{kpc}^3$ and $M(R_{\mathtt{G}}) = 1.7 \times 10^{11}\ M_\odot$ for the former, and $m/T = 180$ eV/^{o}K, $\rho(R_{\mathtt{G}}) = 7.15 \times 10^6\ M_\odot/\text{kpc}^3$ and $M(R_{\mathtt{G}}) = 3.24 \times 10^{11}\ M_\odot$ for the latter. We plot the results of the fits for the parameters m/T, $M(R_{\mathtt{G}})$ and $\rho(R_{\mathtt{G}})$, for $R_{\mathtt{G}}$ ranging from 7.18 kpc to 15 kpc, in figures 13-15. From figure 13, the fitted values for m/T range between 179 and 193 eV/^{o}K. This is to be compared with the result from section 2 of $m/T \sim 191$ eV/^{o}K. The fitted values for M and ρ versus $R_{\mathtt{G}}$ are shown in figures 14 and 15, respectively. The former is monotonically increasing and the latter monotonically decreasing in $R_{\mathtt{G}}$. (The mass and density functions for a self-gravitating isothermal gas go like r and $1/r^2$, respectively, in the limit $r \to \infty$.) From figure 14 and eq. (5), we can numerically integrate $GM(R_{\mathtt{G}})/R_{\mathtt{G}}^2$ in $R_{\mathtt{G}}$ to obtain the gravitational potential function Φ. Then in analogy to what was done in section 2, we can use these results to plot $\log[\rho(R_{\mathtt{G}})/\rho(r_0)]$, here obtained from figure 15, versus $\Phi(R_{\mathtt{G}})$. (We set $r_0 \approx 7.18$ kpc, with $\Phi(r_0) = 0$.) The results are shown in figure 16 for $7.18 \le R_{\mathtt{G}} \le 15$ kpc. As in section 2, one gets an approximate straight line, in agreement with (3). Thus the fitted values for the boundary conditions are consistent with a Boltzmann gas. From figure 16 one gets slope $\approx -2.58 \times 10^{-11}$ kg/J, and upon identifying this with $-m/(k_B T)$, one gets $m/T \approx 200$ eV/^{o}K. Thus, all of the estimates of m/T for the NGC 2841 galactic halo are reasonably close. The small discrepancies between the results found for m/T in this section with that of section 2 should be due in large part to the fact that these estimates were made in different regions of the halo. The upper bound for r used for estimating m/T in section 2 was 22 kpc, while here fits to the Boltzmann gas were performed all the way out to the last data point at $r = 51.6$ kpc. On the other hand, figure 4 shows deviations from a Boltzmann description at very large distances $r >> 22$ kpc (or $\phi > 47 \times 10^{10}$ J/kg).

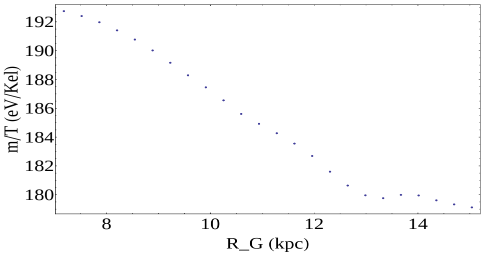

Figure 13: Fitted values of m/T for NGC 2841 for values of $R_{\mathtt{G}}$ between 7.18 and 15 kpc.

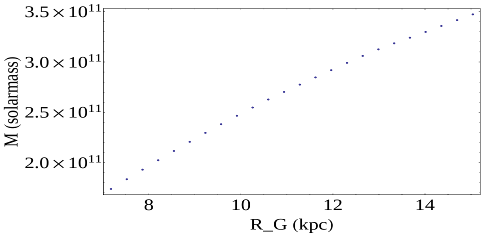

Figure 14: Fitted values of M for NGC 2841 for values of $R_{\mathtt{G}}$ between 7.18 and 15 kpc.

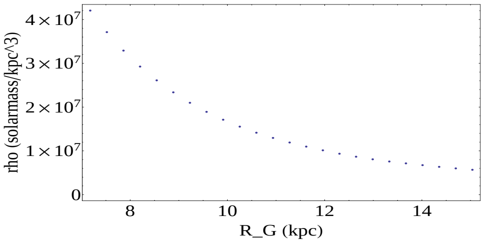

Figure 15: Fitted values of ρ for NGC 2841 for values of $R_{\mathtt{G}}$ between 7.18 and 15 kpc.

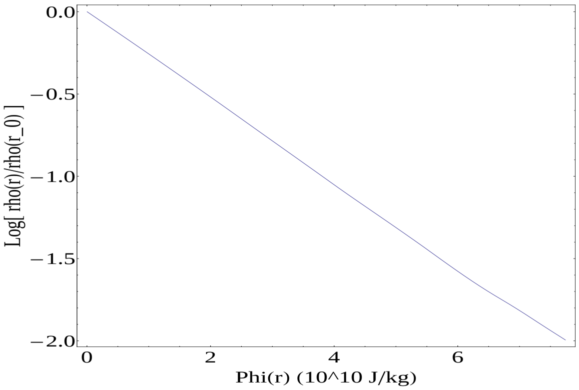

Figure 16: $\log[\rho(R_{\mathtt{G}})/\rho(r_0)]$ versus $\Phi(R_{\mathtt{G}})$ for $r_0 = 7.18 > R_{\mathtt{G}} > 15$ kpc. The slope is approximately $\approx -2.58 \times 10^{-11}$ kg/J, which corresponds to $m/T \approx 200$ eV/^{o}K.

NGC 5055

In section 2, Boltzmann gas-like behavior was observed for the galactic halo of NGC 5055 in the region $10 < r < 25$ kpc. Here we will examine fits of the rotation velocity data to the Boltzmann gas for $R_{\mathtt{G}} \leq r \leq 44.4$ kpc, where $R_{\mathtt{G}}$ ranges from 6.47 to 11.1 kpc. Due to the error bars in the rotation velocity data, fits do not appear to be reliable when the boundary value $R_{\mathtt{G}}$ is larger than 11.1 kpc. A fit of the rotation velocity data to the isothermal gas for the region $r \geq R_{\mathtt{G}} \approx 6.47$ kpc is given in figure 17. The results for this fits are: $m/T = 484$ eV/^{o}K, $\rho(R_{\mathtt{G}}) = 2.7 \times 10^7\ M_\odot/\mathrm{kpc}^3$ and $M(R_{\mathtt{G}}) = 6.05 \times 10^{10}\ M_\odot$. The fitted value for $M(R_{\mathtt{G}})$ is close to the NGC 5055 disk mass of $6.035 \times 10^{10}\ M_\odot$. A reasonable lower bound for $R_{\mathtt{G}}$ is then 6.47 kpc, as it can be associated with an effective size of the baryonic component to the galaxy. The results for the fits for $R_{\mathtt{G}}$ ranging from 6.47 kpc to 11.1 kpc appear in figures 18-20. The fitted values for m/T are plotted in figure 18 and range between 484 and 539 eV/^{o}K. This can be compared with the result of 443 eV/^{o}K obtained in section 2. The gravitational potential function Φ is again obtained by numerically integrating $GM(R_{\mathtt{G}})/R_{\mathtt{G}}^2$, using the mass function in figure 19. In figure 21, this is compared with the log of the density $\rho(r)$, obtained from figure 20. (We have set $\Phi(r_0) = 0$, $r_0 \approx 6.47$ kpc.) The result is once again an approximate straight line, now for the region $6.47 < R_{\mathtt{G}} < 11.1$ kpc, with slope $\approx -5.62 \times 10^{-11}$ kg/J. Upon identifying this with $-m/(k_B T)$, one gets $m/T \approx 435$ eV/^{o}K, which is close to the estimate in section 2.

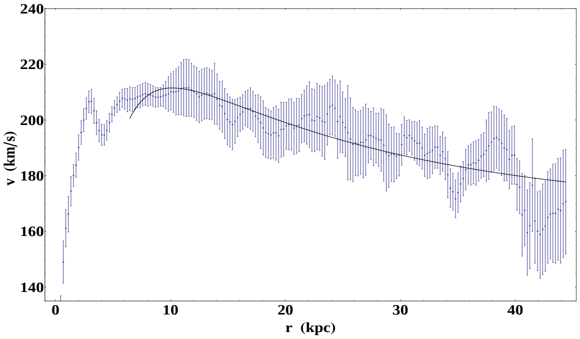

Figure 17: The results for the three-parameter fit of NGC 5055 rotation velocity data for $R_{\mathtt{G}} = 6.47$ kpc are: $m/T = 484$ eV/^{o}K, $\rho(R_{\mathtt{G}}) = 2.7 \times 10^7\ M_\odot/\mathrm{kpc}^3$ and $M(R_{\mathtt{G}}) = 6.05 \times 10^{10}\ M_\odot$.

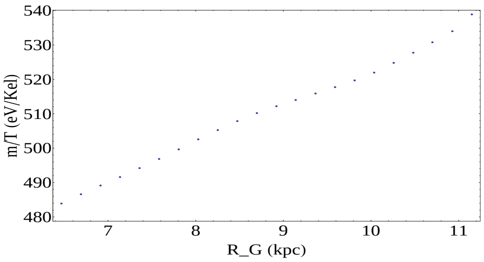

Figure 18: Fitted values of m/T for NGC 5055 for values of $R_{\mathtt{G}}$ between 6.47 and 11.1 kpc.

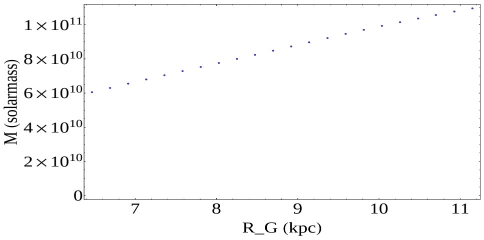

Figure 19: Fitted values of M for NGC 5055 for values of $R_{\mathtt{G}}$ between 6.47 and 11.1 kpc.

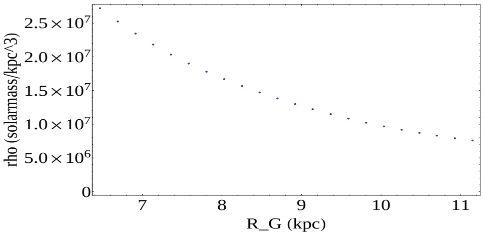

Figure 20: Fitted values of ρ for NGC 5055 for values of $R_{\mathtt{G}}$ between 6.47 and 11.1 kpc.

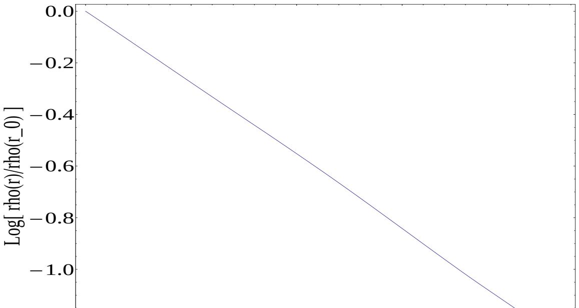

Figure 21: $\log[\rho(R_{\mathtt{G}})/\rho(r_0)]$ versus $\Phi(R_{\mathtt{G}})$ for $r_0 \approx 6.47 > R_{\mathtt{G}} > 11.1$ kpc. The slope is $\approx -5.62 \times 10^{-11}$ kg/J, which corresponds to $m/T \approx 435$ eV/^{o}K.

NGC 3521

In section 2, Boltzmann gas-like behavior was observed for the galactic halo of NGC 3521 in the region $7 < r < 15$ kpc. A fit of the rotation velocity data to the isothermal gas for the region $R_{\mathtt{G}} \approx 7.1$ kpc $\leq r \leq 35.5$ kpc is given in figure 22. The results of the fit are: $m/T = 437$ eV/^{o}K, $\rho(R_{\mathtt{G}}) = 2.45 \times 10^7\ M_\odot/\mathrm{kpc}^3$ and $M(R_{\mathtt{G}}) = 8.8 \times 10^{10}\ M_\odot$. The results of fits for $R_{\mathtt{G}}$ ranging from 7.1 to 13.8 kpc are plotted in figures 23-25. The fitted values for m/T appear in figure 16 and range between 320 and 446 eV/^{o}K. This is to be compared with the result of $m/T \sim 384$ eV/^{o}K obtained in section 2. As before, the gravitational potential function Φ is obtained by numerically integrating $GM(R_{\mathtt{G}})/R_{\mathtt{G}}^2$, using the mass function in figure 24. We plot $\log[\rho(R_{\mathtt{G}})/\rho(r_0)]$ versus $\Phi(R_{\mathtt{G}})$ of figure 26 for $r_0 \approx 7.1 \leq R_{\mathtt{G}} \leq 13.8$ kpc. The result is an approximate straight line. The approximation improves upon restricting the domain to $9.5 < R_{\mathtt{G}} < 12.5$ kpc, as is shown in the inset of figure 26. In that latter region the slope $\approx -7.31 \times 10^{-11}$ kg/J. Upon identifying this with $-m/(k_B T)$, one gets $m/T \approx 566$ eV/^{o}K. Agreement of the different estimates of m/T in this case is not as close as it was for the previous two galaxies. We suspect that this is due in large part to the Boltzmann gas description breaking down for NGC 3521 at distances beyond 15 kpc, as is indicated in figure 8.

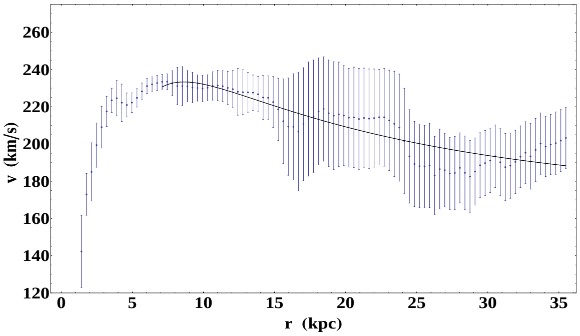

Figure 22: The results for the three-parameter fit of NGC 3521 rotation velocity data for $R_{\mathtt{G}} = 7.1$ kpc are: $m/T = 437$ eV/^{o}K, $\rho(R_{\mathtt{G}}) = 2.45 \times 10^7\ M_\odot/\mathrm{kpc}^3$ and $M(R_{\mathtt{G}}) = 8.8 \times 10^{10}\ M_\odot$.

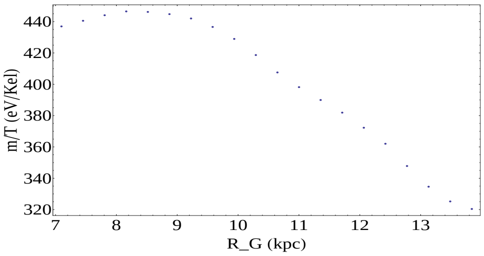

Figure 23: Fitted values of m/T for NGC 3521 for values of $R_{\mathtt{G}}$ between 7.1 and 13.8 kpc.

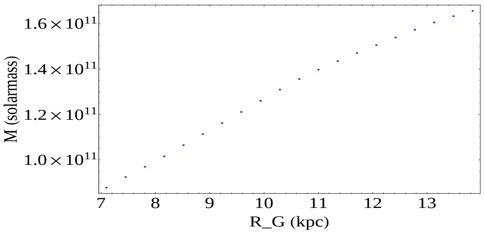

Figure 24: Fitted values of M for NGC 3521 for values of $R_{\mathtt{G}}$ between 7.1 and 13.8 kpc.

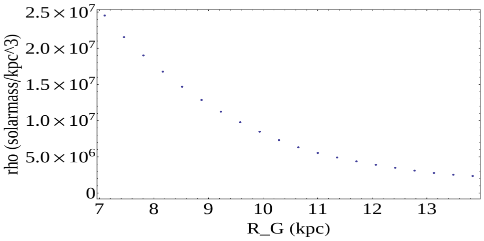

Figure 25: Fitted values of ρ for NGC 3521 for values of $R_{\mathtt{G}}$ between 7.1 and 13.8 kpc.

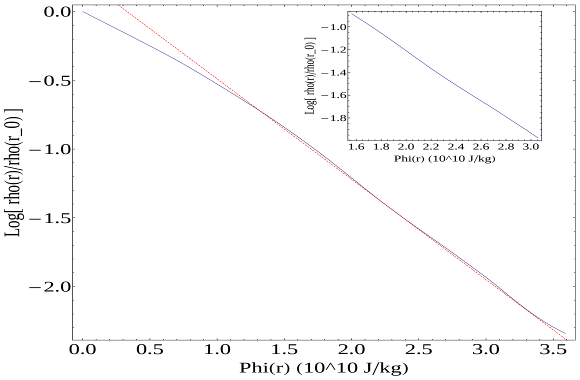

Figure 26: $\log[\rho(R_{\mathtt{G}})/\rho(r_0)]$ versus $\Phi(R_{\mathtt{G}})$ for $r_0 \approx 7.1 > R_{\mathtt{G}} > 13.8$ kpc. It is compared to a straight line (red, dashed) with slope $\approx -7.31 \times 10^{-11}$ kg/J, corresponding to $m/T \approx 566$ eV/^{o}K. The domain is restricted to $9.5 < R_{\mathtt{G}} < 12.5$ kpc in the inset.

NGC 2403

In section 2, Boltzmann gas-like behavior was observed for the galactic halo of NGC 2403 in the region $3 < r < 10$ kpc. Here we do fits of the rotation velocity data to the Boltzmann gas in the region $R_{\mathtt{G}} \leq r \leq 24$ kpc for $R_{\mathtt{G}}$ ranging from 6.5 to 10 kpc. A fit of the rotation velocity data to the isothermal gas for the region $r \geq R_{\mathtt{G}} \approx 6.5$ kpc is given in figure 27. The results for the fit are: $m/T = 752$ eV/^{o}K, $\rho(R_{\mathtt{G}}) = 6.6 \times 10^6\ M_\odot/\mathrm{kpc}^3$ and $M(R_{\mathtt{G}}) = 2.39 \times 10^{10}\ M_\odot$. The fitted value for $M(R_{\mathtt{G}})$ is close to the NGC 2403 disk mass. So it is a reasonable the lower bound for $R_{\mathtt{G}}$. The results for the fits for $R_{\mathtt{G}}$ ranging from 6.5 kpc to 10 kpc appear in figures 28-30. The fitted values for m/T appear in figure 28 and range between 739 and 810 eV/^{o}K, which is a bit lower than the result of $m/T \sim 1085$ eV/^{o}K obtained in section 2. The gravitational potential function Φ is obtained by numerically integrating $GM(R_{\mathtt{G}})/R_{\mathtt{G}}^2$, using the mass function in figure 29. The plot of $\log[\rho(R_{\mathtt{G}})/\rho(r_0)]$ versus $\Phi(R_{\mathtt{G}})$ is shown in figure 31. We restrict the domain further to $6.75 < R_{\mathtt{G}} < 8$ kpc in the inset of figure 31, where the slope $\approx -1.01 \times 10^{-10}$ kg/J. This corresponds to $m/T \approx 786$ eV/^{o}K, which is within the range of values found in figure 28, although not too close to the result of section 2.

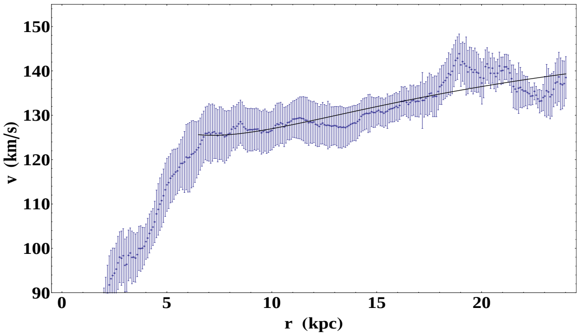

Figure 27: The results for the three-parameter fit of NGC 2403 rotation velocity data for $R_{\mathtt{G}} = 6.5$ kpc are: $m/T = 752$ eV/^{o}K, $\rho(R_{\mathtt{G}}) = 6.6 \times 10^6\ M_\odot/\mathrm{kpc}^3$ and $M(R_{\mathtt{G}}) = 2.39 \times 10^{10}\ M_\odot$.

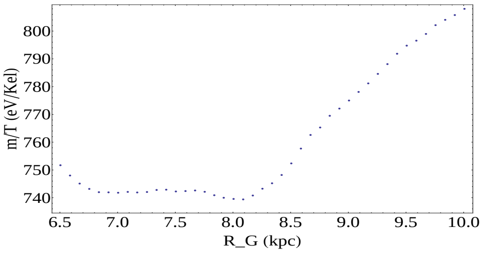

Figure 28: Fitted values of m/T for NGC 2403 for values of $R_{\mathtt{G}}$ between 6.5 and 10 kpc.

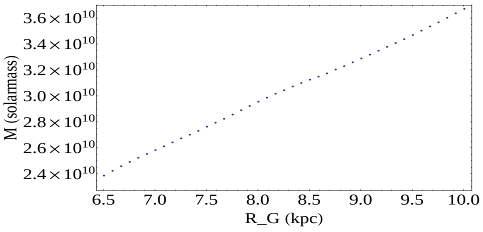

Figure 29: Fitted values of M for NGC 2403 for values of $R_{\mathtt{G}}$ between 6.5 and 10 kpc.

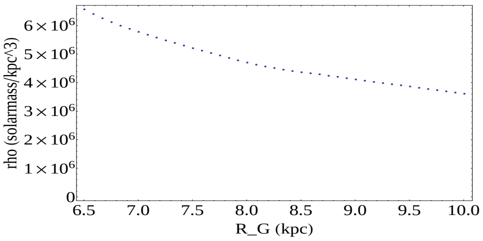

Figure 30: Fitted values of ρ for NGC 2403 for values of $R_{\mathtt{G}}$ between 6.5 and 10 kpc.

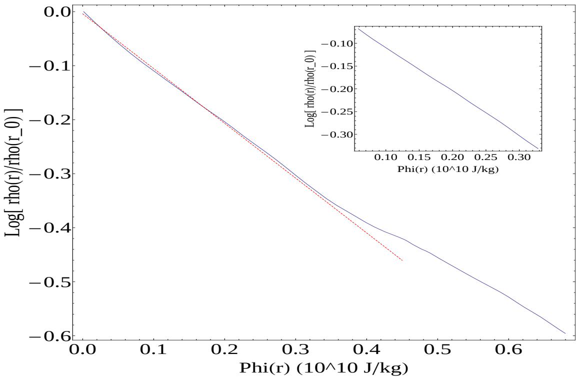

Figure 31: $\log[\rho(R_{\mathtt{G}})/\rho(r_0)]$ versus $\Phi(R_{\mathtt{G}})$ for $r_0 \approx 6.5 > R_{\mathtt{G}} > 9$ kpc. It is compared to a straight line (red, dashed) with slope $\approx -1.01 \times 10^{-10}$ kg/J, which corresponds to $m/T \approx 786$ eV/^{o}K. The domain is restricted to $6.75 < R_{\mathtt{G}} < 8$ kpc in the inset.

4 Concluding Remarks

We examined the rotation velocity data of four galaxies and found that there are substantial regions in the haloes of these galaxies where the behavior is consistent with an isothermal Boltzmann gas. More specifically, using the approximation of spherical symmetry, agreement was found with (3). In section 2, the regions where agreement was found for the haloes of NGC 2841 and NGC 5055 covered a distance of ~ 15 kpc, or roughly four times the distance scale of the disk. (These results and others are summarized in Table 1.) We note that NGC 2841 has the smallest HI gas mass to disk mass ratio (4%) of the four galaxies, and so one should expect the smallest correction in the halo due to the HI gas for NGC 2841. This is in contrast with a HI gas mass to disk mass ratio of 19% for NGC 2403.

In sections 2 and 3, we were able to obtain three independent estimates of m/T for the galactic haloes of NGC 2841, NGC 5055, NGC 3521 and NGC 2403, which are summarized in Table 1. The table also lists the distance scale of the disk in column 2, and the ratio of the HI gas to the disk mass in column 3. Column 4 gives the estimates of m/T found in section 2, which were found from the slope of $\log \rho$ vs the potential. These functions were obtained from direct fits of the rotation velocity data. Column 5 lists values of m/T obtained from fits of the rotation velocity data to the Boltzmann gas in section 3. Column 6 gives the estimates of m/T deduced in section 3 from the boundary values of ρ and M found from fits of the rotational velocity data to the Boltzmann gas. (The domains from which the various determinations were made are shown in parentheses in the table.)

Estimates of m/T (eV/^{o}K)					
Galaxy	R_{disk}	$\frac{M_{HI}}{M_{disk}}$	slope of $\log \rho$ vs ϕ from sec. 2	Boltzmann fits from sec. 3	slope of $\log \rho$ vs ϕ from sec. 3
NGC 2841	3.5 kpc	.04	191 ($7 \leq r \leq 22$ kpc)	$179 - 193$ ($7.18 \leq R_\mathtt{G} \leq 15$ kpc)	200 ($7.18 \leq R_\mathtt{G} \leq 15$ kpc)
NGC 5055	3.622 kpc	.126	443 ($10 \leq r \leq 25$ kpc)	$484 - 539$ ($6.47 \leq R_\mathtt{G} \leq 11.1$ kpc)	435 ($6.47 \leq R_\mathtt{G} \leq 11.1$ kpc)
NGC 3521	3.3 kpc	.11	384 ($7 \leq r \leq 15$ kpc)	$320 - 446$ ($7.1 \leq R_\mathtt{G} \leq 13.8$ kpc)	566 ($9.5 \leq R_\mathtt{G} \leq 12.5$ kpc)
NGC 2403	2.75 kpc	.19	1085 ($3 \leq r \leq 10$ kpc)	$739 - 810$ ($6.5 \leq R_\mathtt{G} \leq 10$ kpc)	786 ($6.75 \leq R_\mathtt{G} \leq 8$ kpc)

Table 1: Three independent determinations of m/T in galactic haloes.

Upon comparing the relative effective temperatures of the four dark matter haloes, we conclude that

$$T_{\mathrm{NGC\,2841}} < T_{\mathrm{NGC\,5055}} \sim T_{\mathrm{NGC\,3521}} < T_{\mathrm{NGC\,2403}}$$

These relative temperatures may not necessarily be correlated with the temperatures of the baryonic matter in the galaxies. In all cases, the Boltzmann form (3) appears to break down at the edges of the halo, both at short and extremely large distances. This is evident from the graphs in section 2. Another signal of the breakdown at very large distances comes from the discrepancies between numericalresults found for m/T in sections 2 and 3. The analysis in section 2 was done for a limited range in r, while the Boltzmann fits carried out in section 3 were performed out to the last data point in r (while we varied the minimum value $R_\mathtt{G}$). The breakdown at extremely large distances may indicate that the dynamics that leads to (3) may not apply at such distances. It is not hard to understand the breakdown at short distances, since the assumptions of spherical symmetry and a single-component gas are not valid approximations close to the disk.

A number of improvements can be performed on the fits of galactic haloes presented here. The most obvious are to drop the assumption of spherical symmetry, and to take into account effects of the HI gas. Furthermore, the restriction of the Poisson equation to the galactic halo may be dropped, and the analysis can be extended to include the galactic core. As densities grow in the interior, it may be useful here to consider the effect of quantum statistics.

Finally, the fact that we find the Boltmann relation (3) to be consistent with rotation velocity data in substantial regions of four galactic haloes may not be accidental. It can be an indication that, even though interactions among dark matter particles are weak, they may be sufficient for the system to settle down to an equilibrium configuration, or perhaps that the gas could achieve equilibrium via random processes arising from gravitational interactions with baryonic matter in thermodynamic contact with a heat bath.

Acknowledgments

We are grateful to Erwin de Blok for providing us with rotation curve data from THINGS. A.S. was supported in part by the DOE, Grant No. DE-FG02-10ER41714.

REFERENCES

[1] W. J. G. de Blok, F. Walter, E. Brinks, C. Trachternach, S-H. Oh and R. C. Kennicutt, Jr., "High-Resolution Rotation Curves and Galaxy Mass Models from THINGS," Astron. J. **136**, 2648 (2008).

[2] S. K. Sarker and A. Stern, "An effective Thermodynamic Description of Galactic Haloes," arXiv:1207.2383 [astro-ph.GA].

[3] B. M. H. R. Wevers, P. C. van der Kruit, and R. J. Allen, A. A. Suppl. Ser. 66, 505 (1986); Begeman, K.G., Ph.D. Dissertation, Rijksuniversiteit Groningen (1987); A. K. Leroy, F. Walter, E. Brinks, F. Bigiel, W. J. G. de Blok, B. Madore and M. D. Thornley, "The Star Formation Efficiency in Nearby Galaxies: Measuring Where Gas Forms Stars Effectively," Astron. J. **136**, 2782 (2008); P. D. Mannheim and J. G. O'Brien, "Fitting galactic rotation curves with conformal gravity and a global quadratic potential," Phys. Rev. D **85**, 124020 (2012).

[4] Emden, R., 'Gaskugeln: Anwendungen der Mechanischen Warmetheorie auf Kosmologische und Meteorologische Probleme', Teubner, Berlin (1907).

[5] F. Walter, E. Brinks, W. J. G. de Blok, F. Bigiel, R. C. Kennicutt, Jr., M. D. Thornley and A. K. Leroy, "THINGS: The HI Nearby Galaxy Survey," Astron. J. **136**, 2563 (2008).